Please do not adjust margins

PCCP

ARTICLE

Probing the Nature of Donor-Acceptor Effects in Conjugated Materials: A Joint Experimental and Computational Study of Model Conjugated Oligomers

Received 00th January 20xx,
Accepted 00th January 20xx

DOI: 10.1039/x0xx00000x

www.rsc.org/

Trent E. Anderson,[a] Evan W. Culver,[a] Irene Badía-Domínguez,[b] Wyatt D. Wilcox,[a] Claire E. Buysse,[a] M. Carmen Ruiz Delgado,[b] and Seth C. Rasmussen*[a]

A series of model oligomers consisting of combinations of a traditional strong donor unit (3,4-ethylenedioxythiophene), a traditional strong acceptor unit (benzo[*c*][1,2,5]thiadiazole), and the ambipolar unit thieno[3,4-*b*]pyrazine were synthesized via cross-coupling methods. The prepared oligomers include all six possible dimeric combinations in order to characterize the extent and nature of donor-acceptor effects commonly used in the design of conjugated materials, with particular focus on understanding how the inclusion of ambipolar units influence donor-acceptor frameworks. The full oligomeric series was thoroughly investigated via photophysical and electrochemical studies, in parrallel with with density functional theory (DFT) calculations, in order to correlate the nature and extent of donor-acceptor effects on both frontier orbital energies and the desired narrowing of the HOMO-LUMO energy gap. The corresponding relationships revealed should then provide a deeper understanding of donor-acceptor interactions and their application to conjugated materials.

Introduction

Although conjugated organic polymers are typically viewed as modern materials, examples date back to the early 1800s.[1,2] The modern era of these materials began with the first reports of their conductive nature in the early 1960s, but it was advances in the 1970s that brought particular focus to these systems with the first report of metallic conductivities.[1,2] Over time, conjugated materials have continued to receive significant interest due to their combination of the electronic and optical properties of classical inorganic semiconductors, with many of the desirable properties of organic plastics.[3,4] This ultimately gave rise to the current field of organic electronics, with focus on technological applications such as sensors, electrochromic devices, organic photovoltaics (OPVs), organic light-emitting diodes (OLEDs), and organic field effect transistors (OFETs).[3-9]

For the applications given above, successful organic semi-conducting materials must combine several critical properties, including processability, stability, high conjugation length, a suitable band gap (E_g), and sufficient charge mobility.[10,11] Of these factors, control of the E_g has been given significant attention. As the E_g is the energetic separation between the filled valence and empty conduction bands, it corresponds to the HOMO-LUMO gap of the bulk, solid-state material, and determines such properties as the onset of absorbance or the energy of any potential emission.[10-18] In addition, as the E_g and the frontier orbitals are intimately related, the ability to control the orbital energy levels allows tuning of both the E_g and the material's redox properties. As such, tuning of the orbital energy levels is also crucial for providing environmental stability, as well as proper matching of energy levels with other electronic components in device applications.[16]

Recent efforts in band gap engineering of conjugated polymers have largely aimed to produce either reduced band gap (E_g = 1.5–2.0 eV)[11,15,16] or low band gap (E_g < 1.5 eV)[11,12,15-18] materials in order to obtain materials which can more efficiently absorb solar radiation for OPV applications. Although various structure-function relationships have been shown to play a role in the resulting E_g of conjugated polymers,[10,11] the successful production of lower E_g materials is primarily limited to either enhancing the quinoidal nature of the polymer backbone or the construction of donor-acceptor (D-A) frame-works.[11-23] Of these two approaches, the D-A framework (Fig. 1) has become the most commonly applied design strategy for the production of lower E_g materials.

First introduced by Havinga and coworkers in 1992,[24,25] the D-A approach was based on the regular alternation of strong donor and acceptor-like groups along the polymer backbone (Fig. 1). One explanation for the lowered E_g of D-A frameworks

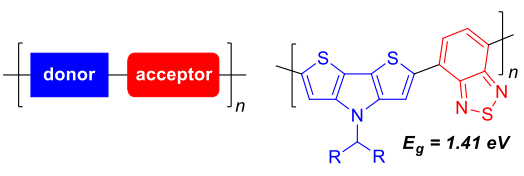

Fig. 1. Conceptual donor-acceptor framework and a simple representative example.

[a] Department of Chemistry and Biochemistry, North Dakota State University, NDSU Dept. 2735, P.O. Box 6050, Fargo, ND 58108, USA. E-mail: seth.rasmussen@ndsu.edu.
[b] Department of Physical Chemistry, University of Málaga, Campus de Teatinos s/n, Málaga 29071, Spain. E-mail: carmenrd@uma.es.

Electronic Supplementary Information (ESI) available: NMR spectra for all compounds, modelling of second order effects in EDOT species, X-ray data for **1** and EDOT-BTD, and additional computational results. See DOI: 10.1039/x0xx00000x

This journal is © The Royal Society of Chemistry 2017

Please do not adjust margins

Please do not adjust margins

has been in terms of reduced bond length alternation. The reasoning here is that providing that the corresponding donor and acceptor units are strong enough, it may be possible to evoke a new resonance form exhibiting double bond character between the donor and acceptor units as shown below:

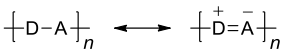

Averaging these two resonance forms would thus reduce bond length alternation along the conjugated backbone, leading to a decreased E_g.[11,19-22] However, the most common explanation for the reduction in E_g is due to hybridization of the frontier orbitals of the donor and acceptor, thus producing a hybrid material with HOMO levels characteristic of the donor and LUMO levels characteristic of the acceptor.[11,19-22] Still, it should be stressed that this model was originally proposed and shown in one class of polymers (polysquaraines/polycroconaines) and has essentially been applied since to all conjugated materials without further modification or refinement. In fact, several theoretical studies have questioned the validity of the theory and have suggested that as the acceptor units applied are typically quinoidal and the donor units are aromatic, it is the geometrical mismatch between quinoidal and aromatic forms which is the important factor, thus resulting in reduced bond length alternation and lower E_g as a consequence.[26-29] Furthermore, the commonly presented orbital diagram consisting of a donor-localized HOMO and an acceptor-localized LUMO is only one of the five possible cases that can occur in D-A copolymers,[30,31] with the molecular orbital localization depending on various factors including the offsets of HOMO and LUMO between the D and A units, the molecular orbital symmetry, and steric effects.[32]

In the application of the D-A model, monomers are typically viewed as an electron-rich donor, an electron-poor acceptor, or a neutral spacer unit. However, this commonly held view has been recently complicated by the realization that the common building block thieno[3,4-*b*]pyrazine (TP)[15,33-37] is not a simple acceptor unit as previously believed, but acts simultaneously as both a donor and acceptor unit.[38] Due to this dual donor and acceptor nature, TPs exhibit a localized intramolecular charge transfer (ICT) transition from a thiophene-localized HOMO to a more pyrazine-localized LUMO (Fig. 2),[34-36] and this dual nature has led us to propose calling such units *ambipolar* building blocks[38] to differentiate them from traditional donors or acceptors. This ambipolar character has now been further demonstrated with the successful generation of low E_g materials via alternating copolymers of nonconventional TP-A pairings,[17,18] as well as the more traditional D-TP materials.[15]

The issues discussed above have led to a realization that the commonly applied D-A approach to the design of reduced and low E_g materials is overly simplistic and does not accurately account for the electronic properties of all D-A materials. As such, it is clear that this theoretical framework needs further development in order to produce meaningful design criteria for the production of conjugated materials with smaller band gaps. In an effort to advance the understanding of the extent and nature of D-A effects in conjugated materials, the current study reports the preparation and study of a series of symmetrical and asymmetrical dimers consisting of combinations of traditional donors, traditional acceptors, and ambipolar TP units, with particular focus on understanding how the inclusion of ambipolar units influence such D-A effects.

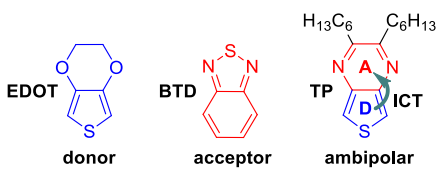

Fig. 2. The monomeric units utilized in the model oligomers.

Results and discussion

Oligomer Design and Synthesis

The chosen oligomers were designed such that a comparative series could be developed to evaluate the differences between both symmetrical dimers (i.e. D-D, A-A) and the various asymmetrical analogues expected to exhibit D-A behaviour. Of critical importance was that the corresponding conjugation length was held constant throughout the series, such that conjugation length effects did not distort the evaluation of D-A interactions when comparing properties between the various oligomers. Thus, all monomeric species were selected such that each building block only contributed a single aromatic ring to the conjugated backbone of the oligomer. At the same time, the corresponding donor and acceptor units needed to be strong enough to ensure significant D-A effects. The selected monomeric units were thus 3,4-ethylenedioxythiophene (EDOT)[21,39] for the traditional donor, benzo[*c*][1,2,5]thiadiazole (BTD)[40,41] for the traditional acceptor, and 2,3-dihexylthieno[3,4-*b*]pyrazine as the ambipolar TP unit (Fig. 2). It should be pointed out that the dialkyl TP analogue was chosen over the unfunctionalized parent due to the fact that the parent TP is less stable during redox processes than its functionalized analogues,[15,33,35] and thus the choice was to avoid any potential complication from this issue of redox stability. In addition, the inclusion of the longer side chains would ensure that solubility would not be an issue for oligomers combining two fused-ring monomeric units.

The symmetrical dimers BTD-BTD and EDOT-EDOT were then prepared via various homocoupling methods[42,43] (Scheme 1), while the remaining members of the chosen oligomeric series were prepared by Stille cross-coupling[44] as outlined in Schemes 1 and 2. The TP-TP dimer was prepared as previously reported.[38] Although the intermediate stannyl-TP **4** could be isolated and purified, this cost a substantial loss in yield due to the high reactivity of **4**. Because of this, **4** was produced and used without isolation, in a manner similar to that previously utilized for the production of TP-TP.[38]

The resulting dimers were all isolated as relatively stable solids, with the more electron-rich systems (EDOT-EDOT, EDOT-TP, TP-TP) exhibiting reduced environmental stability in comparison to the more electron-deficient species. To limit complications when dealing with the more reactive TP-TP dimer, the exterior α-positions were blocked with trimethylsilyl groups (i.e., TMS) to enhance stability. It has been previously shown that the TMS group contributes little to no effect to the corresponding optical or electronic properties.[38]

This journal is © The Royal Society of Chemistry 20xx

Please do not adjust margins

Please do not adjust margins

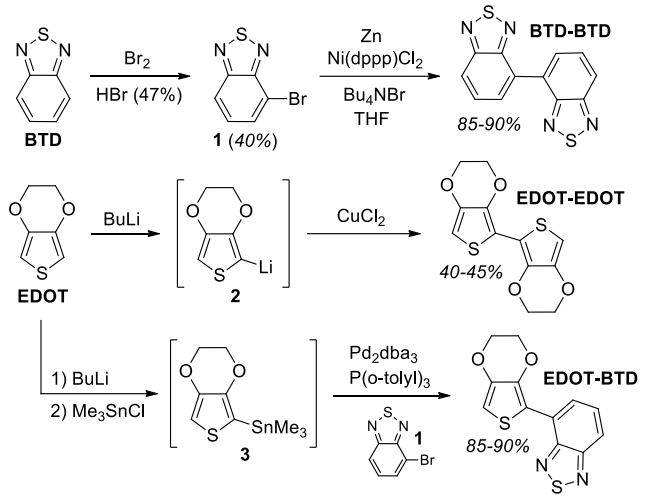

Scheme 1. Synthesis of model dimers of benzo[*c*][1,2,5]thiadiazole (BTD) and 3,4-ethylenedioxythiophene (EDOT).

X-ray crystallography

In order to evaluate potential D-A effects on the dimer geometries, efforts were undertaken to obtain single crystals of EDOT-BTD, EDOT-TP, and TP-BTD. Although these efforts were unsuccessful for the TP-based dimers, EDOT-BTD has been successfully crystallized and its determined structure is shown in Fig. 3. Selected bond distances and angles for EDOT-BTD are given in Table 1, along with those for thiophene[45] and BTD[46] for comparison. The oligomer EDOT-BTD crystallizes in the monoclinic space group $P2_1/c$, with four molecules per unit cell. As expected, the dimer adopts an *anti*-configuration such that the fused rings are oriented on opposite sides of the conjugated backbone. Although the BTD unit is completely planar, there is an 18° rotation along the interannular bond such that the EDOT unit is slightly out of plane.

Comparing the structural parameters of EDOT-BTD to that of thiophene (Table 1) reveals very close agreement between the EDOT unit and thiophene, indicating little change to the EDOT unit upon coupling to the strong electron-acceptor BTD. In comparison to BTD, however, EDOT-BTD does exhibit some small changes in the six-membered ring of the BTD unit. These changes are largely limited to reducing the extent of bond localization within the six-membered ring, resulting in bond lengths more representative of benzene itself. With the exception of the C(8)-C(9) bond fusing the two rings of BTD, the bond lengths are all in relatively good agreement with the terminal phenyl groups of 2,5-diphenylthiophene.[47]

Of particular interest is the nature of the interannular bond C(4)-C(7). As discussed above, some have proposed that the D-A interaction provides a new resonance form exhibiting double bond character between the donor and acceptor units and contributions of this new resonance form would lead to reduced

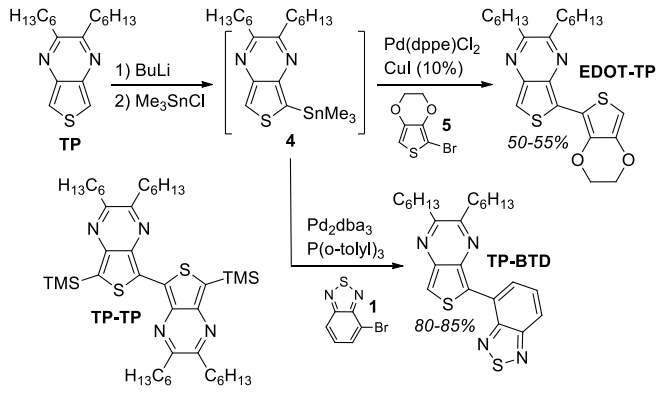

Scheme 2. Synthesis of thieno[3,4-*b*]pyrazine (TP)-based model dimers.

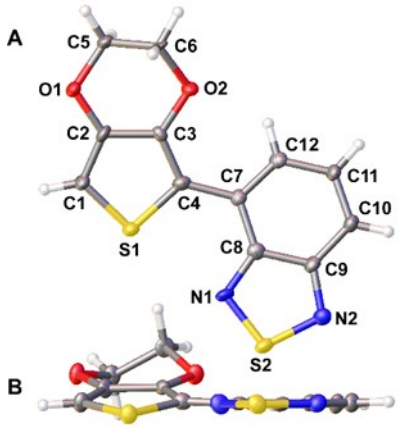

Fig. 3. Face (A) and edge (B) ellipsoid plots of **EDOT-BTD** at the 50% probability level.

Table 1 Selected Experimental Geometric Parameters of EDOT-BTD, thiophene, and BTD.

Parameter	EDOT-BTD	thiophene[a]	BTD[b]
S(1)-C(1)	1.716(6)	1.714	-
S(1)-C(4)	1.735(6)	1.714	-
C(1)-C(2)	1.354(8)	1.370	-
C(2)-C(3)	1.411(8)	1.423	-
C(3)-C(4)	1.376(8)	1.370	-
C(4)-C(7)	1.469(8)	-	-
C(7)-C(8)	1.425(8)	-	1.448
C(7)-C(12)	1.376(8)	-	1.310
C(8)-C(9)	1.451(8)	-	1.418
C(9)-C(10)	1.406(9)	-	1.459
C(10)-C(11)	1.363(8)	-	1.310
C(11)-C(12)	1.421(8)	-	1.478
N(1)-C(8)	1.347(8)	-	1.342
N(1)-S(2)	1.614(5)	-	1.606
S(2)-N(2)	1.624(6)	-	1.613
N(2)-C(9)	1.351(7)	-	1.323
C(1)-S(1)-C(4)	92.9(3)	92.17	-
S(1)-C(1)-C(2)	110.9(5)	111.47	-
C(1)-C(2)-C(3)	113.4(5)	112.45	-
C(2)-C(3)-C(4)	113.7(6)	112.45	-
S(1)-C(4)-C(3)	109.1(5)	111.47	-
S(1)-C(4)-C(7)	122.7(4)	-	-
C(4)-C(7)-C(8)	122.1(6)	-	-
C(7)-C(8)-C(9)	120.5(6)	-	118.04
N(1)-C(8)-C(9)	112.8(5)	-	114.41
N(1)-S(2)-N(2)	101.2(3)	-	101.39
S(2)-N(2)-C(9)	106.2(4)	-	106.24
C(8)-C(9)-C(10)	121.0(5)	-	119.69
C(9)-C(10)-C(11)	117.5(6)	-	119.55
C(10)-C(11)-C(12)	121.8(6)	-	121.09
C(11)-C(12)-C(7)	123.4(5)	-	120.60

Please do not adjust margins

Please do not adjust margins

[a] Ref. 45. [b] Ref. 46.

bond length alternation and thus a lowering of the band gap. Of course, the contribution of such a resonance form should be evidenced by a shortening of the interannular bond between the donor and acceptor corresponding to greater double-bond character. The C(4)-C(7) bond length, however, is 1.469 Å, which is far closer to the length of a non-conjugated single bond (ca. 1.52 Å) than a typical C=C bond (1.35 Å).[48] In fact, this bond is actually longer than the equivalent bond between thiophene and benzene in 2,5-diphenylthiophene (1.439 Å).[47] The lack of any discernible double bond character in the interannular bond of EDOT-BTD, along with the 18° twist between the donor and acceptor units, casts doubt upon the theory that such D-A interactions results in a new resonance form and thus reduced bond length alternation. In fact, at least from this example, the D-A effects appear to have little to no impact on the physical structure.

Intramolecular Effects on Dimer Structures

Although no observed modulation of the interannular bond is found in EDOT-BTD, other intramolecular interactions between the individual units of the asymmetric dimers do play a role in determining structural aspects such as backbone planarity and preferred conformational orientation. For EDOT-BTD, this includes hydrogen-bonding between the C-H in the 5-position of the BTD unit (i.e., C12) and the adjacent oxygen of the EDOT unit (Fig. 4). The C···O distance here is 2.916 Å (estimated H···O distance of 2.267 Å), with a corresponding C-H···O angle of 124.8°. Although this interaction exhibits limited linear character, this is likely a constraint of the dimer geometry, rather than an indication of marginal strength. Nevertheless, both the angle and C···O distance fall within the previously defined parameters for C-H···O hydrogen bonds.[49,50] In fact, the C···O distance falls within the values characteristic of a significant interaction (2.70-3.50 Å)[49] and is shorter than the majority of such documented C-H···O hydrogen bonds (i.e. 3.0-4.0 Å).[50] Lastly, it should be noted that the interannular twist observed in the EDOT-BTD crystal structure may be the result of maximizing the interaction of the hydrogen bond with the oxygen lone pair that does not lie within the plane of the aromatic rings.

Although the TP-BTD dimer lacks X-ray structural data, support for an analogous C-H···N hydrogen bond[51,52] (Fig. 4) can be found in the large downfield shift for the hydrogen at the 5-position of the BTD unit (9.38 ppm in comparison to 8.03 ppm for the isolated BTD unit). It has been previously reported that such C-H···N interactions result in a shift of ca. 0.5-1 ppm,[53-55] with the shift increasing with the strength of the hydrogen bond.[53] Thus, the 1.35 ppm shift observed for TP-BTD is indicative of an especially strong C-H···N hydrogen bond, which is further supported by a density functional theory (DFT)-calculated bond distance

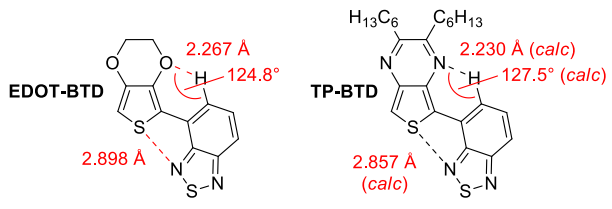

Fig. 4. Intramolecular interactions observed in EDOT-BTD and TP-BTD. The DFT-calculated values for TP-BTD have been computed at the B3LYP/6-311G** level.

of 2.230 Å between the BTD hydrogen and the TP nitrogen, with a corresponding C-H···N angle in TP-BTD of 127.5°. In comparison, the analogous downfield shift observed in the NMR for EDOT-BTD is only 0.30 ppm, which is consistent with the fact that nitrogen is generally a more effective hydrogen acceptor than oxygen.[51] Overall, these NMR results support the fact that these intramolecular hydrogen bonds are not limited to the solid-state structures and also play a role in solution.

In addition to the hydrogen bonding interactions, EDOT-BTD exhibits a S···N contact between the S of the EDOT thiophene and the closest N of the BTD. This S···N contact exhibits a distance of 2.898 Å (less than the sum of the van der Waals radii at 3.35 Å[56]) with a C-S···N angle of 163.3°. Such S···N contacts have been previously observed for thiazole species, although with longer contacts (3.064-3.241 Å).[57,58] Although there is no experimental evidence of this S···N contact in TP-BTD, DFT calculations give a short S···N contact of 2.857 Å and the close structural/electronic similarities of the two thiophene rings would suggest that such a S···N contact likely plays a role in TP-BTD as well. In fact, it is likely that the combination of the two intramolecular attractions accounts for the quite strong energetic preference for the *trans* orientation of the two fused rings as determined by DFT calculations.[17]

Absorption properties

Photophysical data for dimer series are given in Table 2 and UV-vis spectra of the three asymmetric D-A dimers with their respective symmetrical dimers are shown in Fig. 5. The first triad of spectra given in Fig. 5A represents the stereotypical D-A combination, with EDOT and BTD as the respective donor and acceptor units. Here, the D-A combination results in a significant red shift as expected with the low energy absorbance assigned as an ICT transition. This D-A dimer also exhibits a higher energy π–π^* transition of greater intensity, which is consistent with the two-band absorbance commonly seen in D-A

This journal is © The Royal Society of Chemistry 20xx

Please do not adjust margins

Table 2 Photophysical data for the dimer series of EDOT, TP, and BTD units.[a]

[a] Measured from dilute $CHCl_3$ solutions in 1 cm quartz cuvettes. [b] Ref. 38.

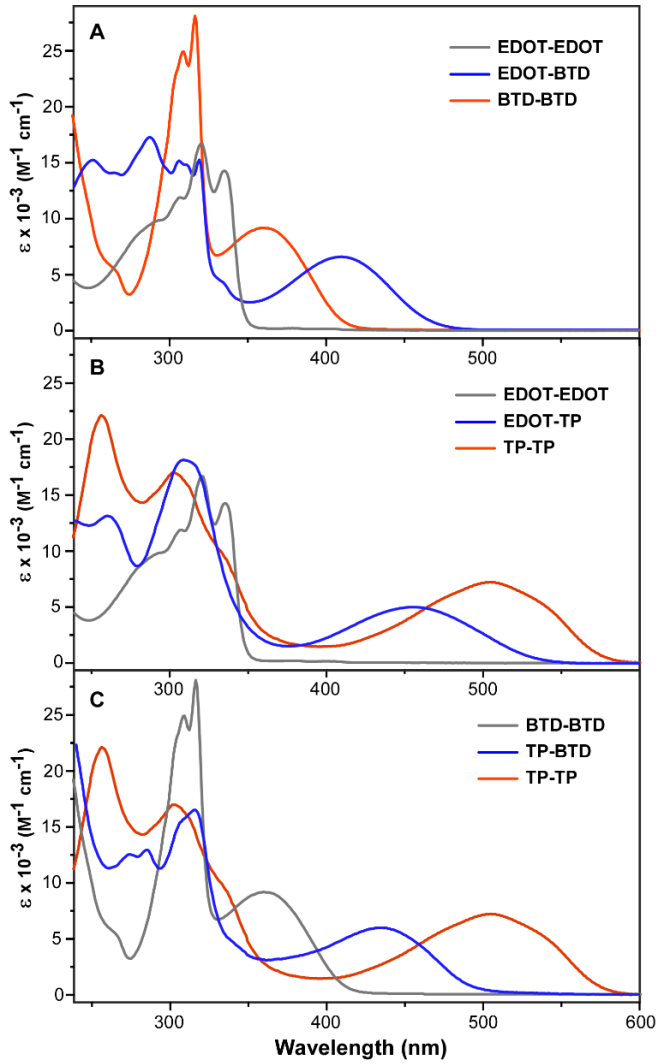

Fig. 5. UV-vis spectra of the symmetrical and asymmetrical model dimers in $CHCl_3$.

frameworks.[21] Although the absorption of the symmetrical dimer of EDOT is as expected, it is interesting to see here that the analogous dimer of BTD does exhibit a lower energy absorption consistent with an ICT transition. Although not observed in the BTD monomer itself, the biphenyl backbone of the BTD dimer provides increased conjugation and greater donor character. The ICT nature of this transition was verified by observed solvatochromism in the associated emission spectra (see SI) and can be assigned to a transition from the biphenyl backbone to the electron-deficient thiadiazole rings, as also verified by TD-DFT calculations (see SI).

The second triad of spectra given in Fig. 5B represents combinations of the traditional donor EDOT with the ambipolar unit TP. Here, the asymmetric EDOT-TP combination results in a significant red shift similar to the previous conventional D-A example, which again would be as assigned as an ICT transition. In comparison to EDOT-BTD, however, the energy of this transition occurs at even lower energy, most likely due to the combined donor ability of both the EDOT and TP units, which should result in a substantially higher energy HOMO level.

Compound	λ_{max}^{abs} (nm)	ε (M^{-1} cm^{-1})	*f*
EDOT-EDOT	296	9000	
	307	10900	
	320	15400	0.50
	335	13200	
BTD-BTD	308	21600	
	316	28600	0.31
	363	9100	0.16
EDOT-BTD	287	17400	0.35
	306	15300	0.48
	319	15400	
	409	6600	0.11
EDOT-TP	260	13300	0.36
	306	17800	0.33
	456	5000	0.11
TP-BTD	274	12300	0.20
	284	12700	
	316	16200	0.17
	435	6000	0.13
TP-TP[b]	257	21800	0.57
	304	17000	0.32
	503	7300	0.15

Replacement of the EDOT unit with another ambipolar TP unit gives an even greater shift to lower energy, as seen for TP-TP. While the donor contributions of EDOT and TP should be similar, the TP dimer would add acceptor contributions from both units, thus resulting in a stabilized LUMO and the observed lower energy transition.

The final triad given in Fig. 5C represents combinations of the ambipolar unit TP with the traditional acceptor BTD. Here, the asymmetric TP-BTD combination results in an ICT transition that is slightly blue-shifted in comparison to the previous EDOT-TP, but still occurs at lower energy than the conventional D-A example of EDOT-BTD. This can be attributed to similar HOMO levels for both TP-BTD and EDOT-BTD, with the ambipolar-acceptor combination providing acceptor contributions from both units and thus a more stabilized LUMO. Again, the symmetrical TP-TP dimer gives the lowest energy ICT transition. Across the full dimer series, the low energy peaks assigned as ICT transitions exhibit oscillator strengths (*f*) of 0.11-0.16 (Table 2), consistent with the reduced allowedness of such transitions.[59] Interestingly, calculated TD-DFT electronic excitations reproduced reasonably well the experimental absorption spectra evolution from the symmetric dimers to their respective asymmetrical D-A dimers (see SI).

Electrochemistry

In order to determine the relative energies of the corresponding frontier orbitals, the electrochemistry of the oligomer series was investigated by cyclic voltammetry (CV). The collected electrochemical data for the full series is given in Table 3 and representative voltammograms are shown in Fig. 6. As typical of thiophene-based oligomers, all species exhibited an irreversible oxidation assigned to the oxidation of the conjugated backbone. For the bulk of the oligomers here, the irreversible nature of the oxidation is attributed to the formation of thiophene-based radical cations that undergo rapid coupling to produce higher oligomeric species. However, as the BTD-BTD dimer does not

Please do not adjust margins

contain a thiophene moiety, it is believed that in this case, oxidation generates a phenylene-based radical cation that can also undergo coupling in a similar manner.

The ability of the ambipolar TP to act as a donor has been previously determined to be on par with that of the conventional donor EDOT.[38] This view of its relative donor strength is further supported here with the oxidation of EDOT-EDOT, EDOT-TP, and TP-TP occurring at nearly identical potentials. In the same way, replacement of EDOT with TP in TP-BTD again give very similar potentials of oxidation.

Table 3 Electrochemical data for the dimer series of EDOT, TP, and BTD units, along with the corresponding DFT-calculated HOMO and LUMO energies.

Compound	E_{pa} (V)[a]	$E_{½}$ (V)[a]	ΔE (mV)	HOMO (eV)			LUMO (eV)		
				Exp[b]	B3LYP[c]	ωB97[d]	Exp[e]	B3LYP[c]	ωB97[d]
EDOT-EDOT	0.49			-5.44	-5.08	-6.69		-1.01	0.89
BTD-BTD	1.58	-1.68	60	-6.56	-6.28	-7.88	-3.50	-2.83	-0.98
EDOT-BTD	0.91	-1.76	80	-5.80	-5.62	-7.49	-3.45	-2.50	-0.53
EDOT-TP	0.49	-1.88	70	-5.43	-5.18	-6.68	-3.30	-2.18	-0.38
TP-BTD	0.93	-1.70	220	-5.85	-5.70	-7.13	-3.55	-2.78	-1.03
TP-TP[f]	0.50	-1.83	110	-5.45	-5.26	-6.58	-3.40	-2.60	-0.91

[a] vs. Ag/Ag+. [b] $E_{HOMO} = -(E_{[onset,ox\ vs.\ Fc+/Fc]} + 5.1)$(eV), Ref. 60. [c] B3LYP/6-311G** [d] optimally tuned ωB97/6-311G**. [e] $E_{LUMO} = -(E_{[onset,red\ vs.\ Fc+/Fc]} + 5.1)$(eV), Ref. 60. [f] Ref. 38.

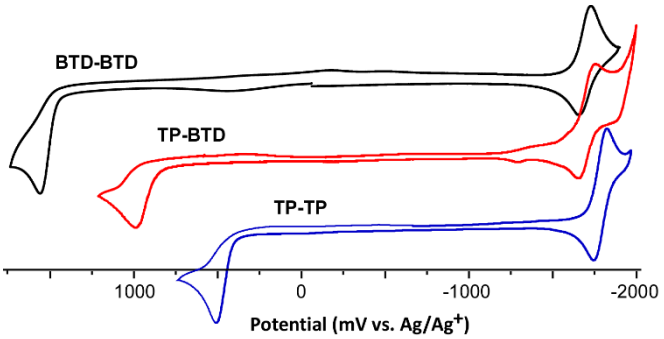

Fig. 6. Cyclic voltammograms of BTD-BTD, TP-BTD and TP-TP (0.1 M Bu_4NPF_6 in CH_3CN).

Comparing the conventional D-A pair EDOT-BTD with the corresponding symmetrical dimers of EDOT or BTD shows that the HOMO energy of EDOT-BTD is not a simple average of the energies of the other two. Rather, the HOMO of EDOT-BTD is higher than the calculated average, which is consistent with the common view that the HOMO of D-A combinations is more characteristic of the donor unit. However, it is still clear that the acceptor unit also contributes significantly to the HOMO, although to a lesser extent.

In addition to the characteristic irreversible oxidation, all dimers besides EDOT-EDOT also exhibit a quasireversible reduction. This reduction is attributed to either the BTD acceptor unit, the electron-deficient pyrazine ring of the TP unit, or various combinations of these in those dimers containing multiple BTD and/or TP units. This assignment is supported by the fact that the only dimer not exhibiting this reduction is also the only one without either BTD or TP content, and by the fact that the reduction of EDOT-TP occurs at a similar potential (within ca. 100 mV) to that of the isolated TP monomer.[33] As those dimers containing two electron-deficient units (BTD-BTD, TP-BTD, TP-TP) exhibit reductions at lower negative potential than either EDOT-BTD or EDOT-TP, it is viewed that the dimer LUMO in those cases must be the result of hybridization of the two electron-deficient units, thus resulting in additional stabilization. This is further supported by the fact that the observed reduction potentials track with the corresponding combined acceptor strengths, as demonstrated in Fig. 6.

DFT Calculations

DFT calculations were then used to gain further insight into the nature and relative energies of the frontier orbitals in the various dimeric combinations investigated above. With the exception of BTD-BTD and EDOT-BTD, all calculated structures were fully planar. The deviations in planarity for the two exceptions were either due to steric effects (BTD-BTD) or competing intramolecular interactions (EDOT-BTD) as discussed above (see SI for the calculated interannular torsional angles). The calculated frontier molecular orbitals for the symmetrical dimers are given in Fig. 7, which depict HOMOs primarily localized to the conjugated bithienyl or biphenyl backbone in all cases. As to be expected, the LUMO for the EDOT dimer was again localized within the conjugated backbone, although the other two cases exhibited fully delocalized LUMOs that fully encompassed the electron-deficient rings. As such, this is in full agreement with the

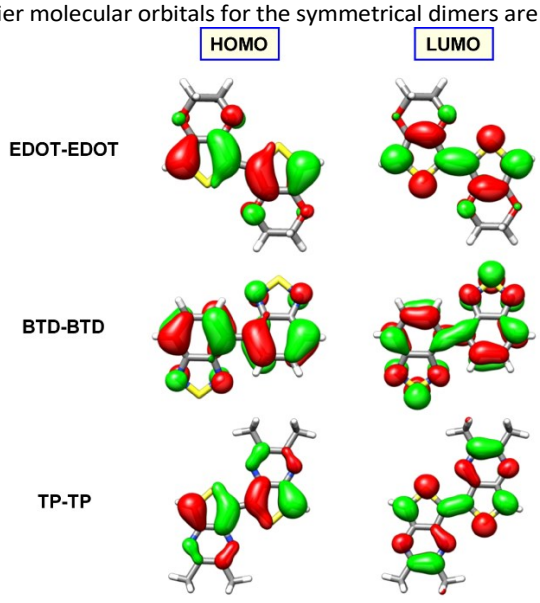

Fig. 7. Frontier molecular orbital topologies (isovalue surface 0.03 a.u.) for the symmetrical D-D and A-A dimers, calculated at the B3LYP/6-311G** level.

This journal is © The Royal Society of Chemistry 20xx

Please do not adjust margins

experimentally determined ICT transitions for BTD-BTD and TP-TP, with such charge transfer absent in EDOT-EDOT.

The calculated frontier molecular orbitals of asymmetrical D-A dimers are given in Fig. 8, which again depict HOMOs primarily localized to the conjugated backbone. The delocalization of the HOMO across both units again reinforces the fact that the donor unit alone does not dictate the HOMO, even if its contribution is greater than that for the acceptor unit.

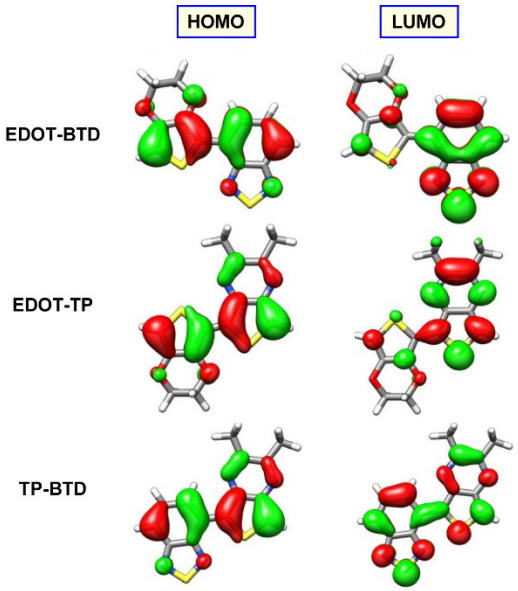

Fig. 8. Frontier molecular orbital topologies (isovalue surface 0.03 a.u.) for the asymmetrical D-A dimers, calculated at the B3LYP/6-311G** level.

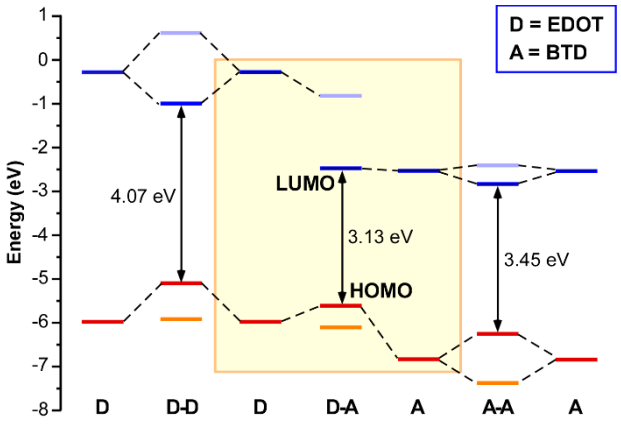

Fig. 9. DFT-calculated (B3LYP/6-311G**) frontier orbital energy levels for combinations of EDOT and BTD.

In the case of both of the EDOT-containing dimers, the LUMO is mainly localized on either the BTD or TP unit, thus supporting the common view that the LUMO is localized on the acceptor in D-A systems. For the final TP-BTD dimer, however, the LUMO is delocalized across both units, with slightly more contribution from the more electron-deficient BTD unit. As with the cases of BTD-BTD and TP-TP, such delocalization supports the previously proposed view that the LUMO results from hybridization of both electron-deficient units in these cases.

The frontier molecular orbital energies for the monomers EDOT and BTD, along with their dimeric combinations, were then calculated and are plotted in Fig. 9. One of the first things revealed here is that the energy diagram for the conventional D-A pair EDOT-BTD (shown in the central box) looks very little like the numerous pictorial representations given in the literature to account for the reduced bandgap in D-A systems.[19,20,22,61,62]

While most literature representations usually show equivalent mixing of the HOMO and LUMO, the LUMO levels are typically too energetically and spatially separated to see substantial mixing in the initial D-A dimer, particularly in the cases of strong acceptors.[63] This is in fact the case here in which the LUMO of EDOT-BTD is essentially unchanged from the BTD monomer, which is also consistent with highly localized LUMO of EDOT-BTD given in Fig. 8. Secondly, while the HOMO-LUMO energy of the D-A pair is certainly lower than that of either the D-D or A-A pair,

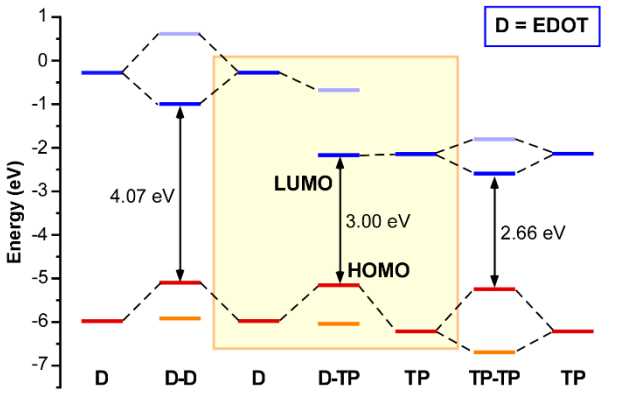

Fig. 10. DFT-calculated (B3LYP/6-311G**) frontier orbital energy levels for combinations of EDOT and TP.

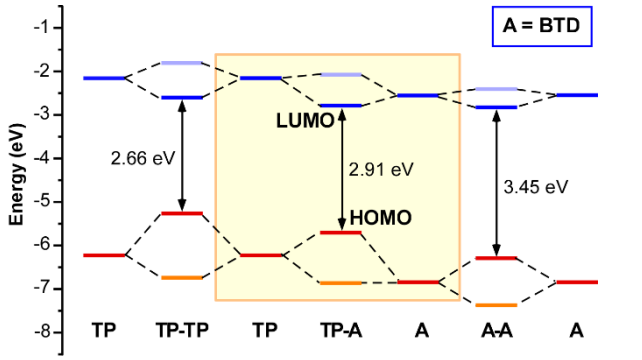

Fig. 11. DFT-calculated (B3LYP/6-311G**) frontier orbital energy levels for combinations of TP and BTD.

the greatest reduction in energy is in comparison to the D-D pair, with only modest reduction in comparison to the A-A pair. Of course, as D-A systems are most often compared directly to their analogous donor homopolymers, this tends to inflate the overall effect of the D-A framework.

The effect of using the ambipolar TP as the acceptor in a D-A pair can then be seen in the analogous molecular orbital energy diagram for combinations of the monomers EDOT and TP, given in Fig. 10. At first glance, Fig. 10 looks quite similar to Fig. 9, particularly in terms of the LUMOs, which again exhibits no real

Please do not adjust margins

mixing in the asymmetric D-A pair. However, the very similar donor strengths of EDOT and TP results in nearly equivalent HOMO levels for all three dimeric combinations, all in excellent agreement with the electrochemical data previously given in Table 3. The fact that the asymmetric EDOT-TP pair does not effectively result in destabilization of the HOMO, coupled with the isolated LUMO on the TP (and thus no LUMO stabilization), actually results in an increase in HOMO-LUMO energy in compari-son to the symmetric TP-TP dimer. This trend in HOMO-LUMO energies and the destabilized LUMO of EDOT-TP in comparison to TP-TP are both in good agreement with the absorption and electrochemical data given in Fig. 5 and Tables 2 and 3.

Finally, the effect of using the ambipolar TP as the primary donor in a D-A pair can then be seen in the energy diagram given in Fig. 11 for combinations of TP and BTD. As the donor strength of TP has already been established to be similar to that of EDOT,[38] it is not surprising that the HOMO energies shown in Fig. 11 are nearly the same as those given in Fig. 9. Unlike the previous cases, however, the inclusion of acceptor properties in both monomer units allows complimentary monomer LUMOs of suitable energies, thus allowing mixing to produce a D-A unit with a de-localized LUMO. As such delocalization also results in stabilization of the D-A LUMO energy, the resulting HOMO-LUMO energy of TP-BTD is reduced in comparison to the analogous EDOT-BTD (Fig. 9). Again, the trends in both the calculated orbital energies and the resulting HOMO-LUMO separations are in excellent agreement with the previous absorption and electro-chemical data given in Tables 2 and 3, as well as illustrated in Fig. 5 and 6.

Experimental methods

Unless noted, all materials were reagent grade and used without further purification. Benzo[*c*][1,2,5]thiadiazole,[64] 2-bromo-3,4-ethylenedioxythiophene (**5**),[65] 2,3-dihexylthieno[3,4-*b*]pyrazine,[33,35] and 2,2',3,3'-tetrahexyl-7,7'-bis(trimethylsilyl)-5,5'-bis(thieno[3,4-*b*]pyrazine) (TP-TP)[38] were prepared as previously described. Commercial EDOT was dissolved in hexanes, dried with $MgSO_4$, filtered and the solvent removed by rotary evaporation. The dried EDOT was then stored cold under N_2 in order to minimize any unwanted impurities via oxidative coupling. The Pd complexes tris(dibenzylideneacetone)dipalladium(0) ($Pd_2(dba)_3$), dichloro[1,2-bis(diphenylphosphino)ethane]palladium(II) (Pd(dppe)Cl_2), and dichloro[1,2-bis(diphenylphosphino)ethane]palladium(II) (Pd(dppp)Cl_2) were stored in a desiccator to reduce any advantageous water content. Dry tetrahydrofuran (THF) and toluene were obtained via distillation over sodium/ benzophenone. Dry CH_3CN was obtained via distillation over CaH_2. *N,N*-Dimethylformamide (DMF) was dried by passing through a silica plug. Zinc powder was cleaned with a dilute hydrochloric acid solution prior to use. All glassware was oven-dried, assembled hot, and cooled under a dry nitrogen stream before use. Transfer of liquids was carried out using standard syringe techniques and all reactions were performed under dry N_2. Chromatographic separations were performed using standard column chromatography methods with silica gel (230-400 mesh), unless otherwise stated. Melting points were determined using a digital thermocouple with 0.1 °C resolution. ^{1}H and ^{13}C NMR spectra were recorded in $CDCl_3$ on a 400 MHz spectrometer and referenced to the chloroform signal. HRMS (ESI-TOF) was performed in house.

4-Bromobenzo[*c*][1,2,5]thiadiazole (1). The following is a modification of previously reported methods.[66] BTD (1.98 g, 14.5 mmol) was added to 145 mL of 47% HBr and the mixture was heated to reflux with stirring. Bromine (0.75 mL, 14.5 mmol) was then added dropwise. After addition, the heating was continued for 1 h, water was added, and the organic phase was extracted with chloroform. The organic layers were combined, dried with $MgSO_4$, and concentrated by rotary evaporation to give a solid powder. The crude mixture was then purified via steam distillation[67] resulting in the isolation of a mixture of **1** and unreacted BTD. Recrystallization of this mixture in methanol gave **1** as a white powder (35-40% yield). mp 78.1-78.8 °C (lit.[66] 80-81°C). ^{1}H NMR: δ 7.98 (dd, *J* = 0.8, 8.8 Hz, 1H), 7.85 (dd, *J* = 0.8, 7.2 Hz, 1H), 7.49 (dd, *J* = 7.2, 8.8 Hz, 1H). ^{13}C NMR: δ 154.6, 153.4, 132.0, 130.0, 120.9, 114.4.

4,4'-Bis(benzo[*c*][1,2,5]thiadiazole) (BTD-BTD). The following is a modification of previously reported methods.[42] Zinc powder (0.38 g, 5.7 mmol), Ni(dppp)Cl_2 (0.607 g, 1.12 mmol), and Bu_4NBr (0.122 g, 0.378 mmol) were added to 10 mL of THF and stirred under N_2. Compound **1** (0.830 g, 3.86 mmol) was then added and the mixture was heated at reflux for 6 h. The solvent was removed under reduced pressure and the crude product was purified via silica chromatography with CH_2Cl_2 as the eluent to give a light yellow solid (85-90% yield). mp. 240.4-241.4 °C (lit.[68] 240-241 °C). ^{1}H NMR: δ 8.27 (dd, *J* = 1.0, 7.0 Hz, 2H), 8.12 (dd, *J* = 1.0, 8.8 Hz, 2H), 7.81 (dd, *J* = 7.0, 8.8 Hz, 2H). ^{13}C NMR: δ 155.5, 153.6, 130.8, 130.0, 129.5, 121.7. NMR data agree well with previously reported values.[68-70]

2,2'-Bis(3,4-ethylenedioxythiophene) (EDOT-EDOT). The following is a modification of previously reported methods.[43] EDOT (1.02 g ,7.18 mmol) was dissolved in 20 mL dry THF, after it was stirred while evacuating and backfilling with N_2 three times. The solution was then cooled to -78 ˚C and BuLi (3.0 mL, 2.5 M) was added dropwise over a span of 10 min, keeping the temperature below -70 °C. Once the BuLi was completely added, the mixture was warmed to 0 ˚C and stirred for 2 h. Anhydrous $CuCl_2$ (1.415 g, 10.5 mmol) was then added and the mixture stirred for 18 h. The solution was then filtered, and solvent removed under reduced pressure. The crude product purified via silica chromatography with CH_2Cl_2-hexanes (1:1 v/v) as the eluent to yield 0.44 g of a white solid (43% yield). mp. 212.1-213.1 °C (lit.[71] 183-185 °C). ^{1}H NMR: δ 6.29 (s, 2H), 4.35 (ddd, *J* = 1.9, 5.3, 6.2 Hz, 4H), 4.26 (ddd, *J* = 1.9, 5.3, 6.2 Hz, 4H). ^{13}C NMR: δ 141.2, 137.0, 109.9, 97.5, 65.0, 64.6. NMR data agree well with previously reported values.[43]

4-(3,4-Ethylenedioxythiophen-2-yl)benzo[*c*][1,2,5]thiadiazole (EDOT-BTD). EDOT (0.21 mL, 2.0 mmol) was dissolved in dry THF (80 mL) and cooled to -78 °C in an acetone-dry ice bath. BuLi (0.88 mL, 2.5 M in hexanes, 2.2 mmol) was added and the mixture stirred for 30 min. Me_3SnCl (2.2 mL, 1.0 M in THF, 2.2 mmol) was then added and stirred for 30 min. The mixture was then allowed to warm to room temperature and stirring was continued for an additional 2 h. The reaction was then concen-

 This journal is © The Royal Society of Chemistry 20xx

Please do not adjust margins

Please do not adjust margins

trated by rotary evaporation to give intermediate **3**, which was used directly without isolation or further purification. Compound **1** (0.43 g, 2.0 mmol), $Pd_2(dba)_3$ (0.037 g, 2 mol%), and P(*o*-tolyl)$_3$ (0.049 g, 8 mol%) were then added to the flask and placed again under N_2. Toluene (60 mL) was added and the solution was heated to 98 °C for 20 h. Water was then added and the organic phase was extracted with $CHCl_3$. The organic layers were combined, dried with $MgSO_4$, and concentrated by rotary evaporation. The crude product was then purified via silica chromatography with an ethyl acetate-hexane (5:95 v/v) mixture as the eluent, to give an orange crystalline product (85-90% yield). mp. 78.1-78.8 °C. ^{1}H NMR: δ 8.33 (dd, *J* = 7.1, 1.0 Hz, 1H), 7.86 (dd, *J* = 8.8, 1.0 Hz, 1H), 7.64 (dd, *J* = 8.8, 7.1 Hz, 1H), 6.59 (s, 1H), 4.42 (ddd, *J* = 2.3, 3.5, 6.3 Hz, 2H), 4.33 (ddd, *J* = 2.3, 3.5, 6.3 Hz, 2H). ^{13}C NMR: δ 155.3, 152.2, 141.7, 126.3, 126.1, 119.0, 113.3, 103.3, 65.0, 64.4. HRMS: m/z 298.9933 [M+Na]+ (calcd. for $C_{12}H_8N_2NaO_2S_2$ 298.9925).

2,3-Dihexyl-5-(trimethylstannyl)thieno[3,4-*b*]pyrazine (4). TP (0.61 g, 2.0 mmol) was dissolved in dry THF (60 mL) and cooled to -78 °C with an acetone-dry ice bath. BuLi (0.88 mL, 2.5 M in hexanes, 2.2 mmol) was added and the mixture was stirred for 30 min. Me_3SnCl (2.2 mL, 1.0 M in THF, 2.2 mmol) was added and stirring was continued for 30 min. The mixture was then allowed to warm to room temperature and stirring was continued for an additional 2 h. The solution was then concentrated by rotary evaporation and purified via a triethylamine-deactivated silica gel column chromatography using 3% diethyl ether in hexane (45% yield). ^{1}H NMR: δ 8.03 (s, 1H), 2.88 (t, *J* = 7.6 Hz, 2H), 2.86 (t, *J* = 7.6 Hz, 2H), 1.86 (p, *J* = 7.6 Hz, 2H), 1.77 (p, *J* = 7.6 Hz, 2H), 1.45-1.55 (m, 4H), 1.35-1.45 (m, 8H), 0.91 (t, *J* = 7.1 Hz, 3H), 0.90 (t, *J* = 7.1 Hz, 3H), 0.49 (s, 9H). ^{13}C NMR: δ 155.8, 149.1, 142.8, 131.0, 122.1, 179.8, 35.7, 34.9, 31.9, 31.7, 29.5, 29.1, 28.4, 27.0, 22.7, 22.6, 14.1(1), 14.0(6), -7.9.

5-(3,4-Ethylenedioxythiophen-2-yl)-2,3-dihexylthieno[3,4-*b*]-pyrazine (EDOT-TP). TP (0.61 g, 2.0 mmol) was dissolved in dry THF (60 mL) and cooled to -78 °C with an acetone-dry ice bath. BuLi (0.88 mL, 2.5 M in hexanes, 2.2 mmol) was added and the mixture was stirred for 30 min. Me_3SnCl (2.2 mL, 1.0 M in THF, 2.2 mmol) was added and stirring was continued for 30 min. The mixture was then allowed to warm to room temperature and stirring was continued for an additional 2 h. The reaction was then concentrated by rotary evaporation to give intermediate **4**, which was used directly without isolation or further purifi-cation. Compound **5** (0.49 g, 2.2 mmol), Pd(dppe)Cl_2 (0.12 g, 10 mol%), and CuI (0.038 g, 10 mol%) were then added to the flask and placed again under N_2. Toluene (60 mL) was added to the flask and the solution was heated at 98 °C for 20 h. Water was then added and the organic phase was extracted with $CHCl_3$. The organic layers were combined, dried with $MgSO_4$, and concentrated by rotary evaporation. The crude product was then purified via silica chromatography with an ethyl acetate-hexane (5:95 v/v) mixture as the eluent, to give an orange crystalline product (50-55% yield). mp. 81.7-82.4 °C. ^{1}H NMR: 7.58 (s, 1H), 6.42 (s, 1H), 4.44 (ddd, *J* = 2.1, 5.0, 6.5 Hz, 2H), 4.30 (ddd, *J* = 2.1, 5.0, 6.5 Hz, 2H), 2.93 (t, *J* = 7.1 Hz, 2H), 2.88 (t, *J* = 7.1 Hz, 2H), 1.99 (p, *J* = 7.1 Hz, 2H), 1.77 (p, *J* = 7.1 Hz, 2H), 1.55-1.25 (m, 12H), 0.91 (t, J = 7.1 Hz, 3H), 0.90 (t, *J* = 7.1 Hz, 3H). ^{13}C NMR: δ 159.6, 156.6, 146.7, 141.2, 138.2, 133.2, 115.9, 111.7, 100.6, 65.4, 64.7, 35.6, 35.0, 32.0, 31.7, 29.7, 29.4, 28.2, 27.0, 22.7, 22.6, 14.2, 14.1. HRMS: m/z 445.1968 [M+] (calcd $C_{24}H_{32}N_2O_2S_2$ 445.1983).

4-(2,3-Dihexylthieno[3,4-*b*]pyrazin-5-yl)benzo[*c*][1,2,5]thiadiazole (TP-BTD). Intermediate **4** was prepared as described for EDOT-TP above. Compound **1** (0.43 g, 2.0 mmol), $Pd_2(dba)_3$ (0.037 g, 2 mol%), and P(*o*-tolyl)$_3$ (0.049 g 8 mol%) were then added to the flask and placed again under N_2. Toluene (60 mL) was added to the flask and the solution was heated to 98 °C for 20 hours. Water was then added and the organic phase was extracted with $CHCl_3$. The organic layers were combined, dried with $MgSO_4$, and concentrated by rotary evaporation. The crude product was then purified via silica chromatography with an ethyl acetate-hexane (5:95 v/v) mixture as the eluent, to give an orange crystalline product (80-85% yield). mp. 102.9-103.5 °C. ^{1}H NMR: 9.38 (dd, *J* = 0.9, 7.3 Hz, 1H), 7.99 (s, 1H), 7.94 (dd, *J* = 0.9, 8.7 Hz, 1H), 7.76 (dd, *J* = 7.3, 8.7 Hz, 1H), 3.00 (t, J = 7.5 Hz, 2H), 2.93 (t, *J* = 7.7 Hz, 2H), 1.96 (p, *J* = 7.5 Hz, 2H), 1.83 (p, *J* = 7.7 Hz, 2H), 1.60-1.35 (m, 12H), 0.94 (t, *J* = 7.1 Hz, 3H), 0.92 (t, *J* = 7.0 Hz, 3H). ^{13}C NMR: δ 156.4, 155.9, 155.3, 152.4, 142.5, 139.7, 130.2, 128.1, 127.0, 126.8, 119.6, 117.8, 35.6, 35.3, 31.9, 31.7, 29.5, 29.2, 28.2, 27.5, 22.7, 22.6, 14.2, 14.1. HRMS: m/z 439.1981 [M+] (calcd $C_{24}H_{30}N_4S_2$ 439.1990).

X-ray Diffraction

X-ray quality crystals of **1** and EDOT-BTD were obtained by vapor diffusion with diethyl ether as the solvent and methanol as the anti-solvent. The X-ray intensity data of the crystals were measured at either 273 or 100 K on a CCD-based X-ray diffractometer system equipped with a Cu X-ray tube (λ = 1.54178 Å) operated at 2000 W of power. The detector was placed at a distance of 5.047 cm from the crystal. Frames were collected with a scan width of 0.3° in ω and exposure time of 10 s/frame and then integrated with the Bruker SAINT software package using an arrow-frame integration algorithm. The unit cell was determined and refined by least-squares upon the refinement of XYZ-centeroids of reflections above 20σ(I). The structure was refined using the Bruker SHELXTL (Version 5.1) Software Package.

Crystal data for 1. $C_6H_3BrN_2S$, M = 215.07, triclinic, *a* = 7.1075(10) Å, *b* = 7.1970(12) Å, *c* = 7.6350(10) Å, *V* = 339.06(9) Å^3, T = 293.15 K, space group P-1, *Z* = 2, 6734 reflections measured, 1192 unique (R_{int} = 0.0414) which were used in all calculations. The final wR_2 was 0.0769 (all data).

Crystal data for EDOT-BTD. $C_{12}H_8N_2O_2S_2$, M = 276.32, monoclinic, *a* = 3.8786(6) Å, *b* = 21.357(2) Å, *c* = 13.401(2) Å, *V* = 1103.4(3) Å^3, T = 100(2) K, space group P 1 21/c 1, *Z* = 4, 6106 reflections measured, 1929 unique (R_{int} = 0.1397) which were used in all calculations. The final wR_2 was 0.2239 (all data).

Theoretical Methodology

Calculations were performed at the density functional theory level using the Gaussian 16 program package.[72] The time-dependent DFT (TD-DFT) approach[73,74] was used to calculate the vertical electronic excitation energies. All DFT and TD-DFT calculations were performed

Please do not adjust margins

Please do not adjust margins

using the global hybrid B3LYP[75,76] functional and the long-range corrected ωB97[77] functional with gap-tuned range-separation parameters using a procedure described in the literature,[78] in conjunction with the 6-311G** basis set.[79,80] For all model oligomers, the alkyl groups were shortened to methyl groups to save computational time. All geometrical parameters were allowed to vary independently apart from planarity of the rings and no symmetry restrictions were applied. On the resulting ground-state optimized geometries, harmonic frequency calculations were performed at the same level of theory to ensure finding the global minimum. Orbital pictures were produced with Chemcraft software.[81]

Absorption Spectroscopy

UV-vis spectroscopy was performed on a dual beam scanning UV-vis-NIR spectrophotometer using samples prepared as dilute $CHCl_3$ solutions in quartz cuvettes. Spectroscopy solvents were dried over molecular sieves prior to use. Oscillator strengths were determined from the visible spectra via spectral fitting to accurately quantify the area of each transition and then calculated using literature methods.[82]

Electrochemistry

All electrochemical methods were performed utilizing a three-electrode cell consisting of platinum disc working electrode, a platinum wire auxiliary electrode, and a Ag/Ag^+ reference electrode (0.251 V vs. SCE).[83] Supporting electrolyte consisted of 0.10 M tetrabutylammonium hexafluorophosphate ($TBAPF_6$) in dry CH_3CN. Solutions were deoxygenated by sparging with argon prior to each scan and blanketed with argon during the measurements. All measurements were collected at a scan rate of 100 mV/s. E_{HOMO} and E_{LUMO} values were estimated from the onsets of the first oxidation or reduction in relation to ferrocene (50 mV vs. Ag/Ag^+), using the value of 5.1 eV vs. vacuum for ferrocene.[60]

Conclusions

In an effort to advance understanding of the extent and nature of D-A effects in conjugated materials, combinations of traditional donors, traditional acceptors, and ambipolar TP units were used to prepare a series of symmetrical and asymmetrical dimers of equivalent conjugation length. Characterization via structural, spectroscopic, and electrochemical methods, along with DFT calculations, then revealed a number of important points. For example, structural analysis found no support for the common belief that D-A combinations result in double bond character between the donor and acceptor units, thus resulting in reduced bond length alternation. As such, the reduced HOMO-LUMO energies in D-A systems appear to be primarily due to the hybridization of the frontier orbitals of the corresponding D and A units, with the LUMO usually localized on the acceptor unit. While results support the view that the donor is the dominant contributor to the HOMO, the acceptor still fully contributes and thus the HOMO is typically delocalized along the conjugated backbone. Due to the asymmetric nature of the HOMO vs. LUMO, ICT processes thus play important roles in these frameworks as commonly invoked.

A primary goal of this study was to provide further insight into the effect of ambipolar units in D-A frameworks, which has revealed that the traditional D-A view is only appropriate when limited to units without any ambipolar character. As shown here, the strong donor character of the ambipolar unit TP would dominate when paired with most traditional donors, resulting in deviations from the accepted view of the D-A model. Even when paired with a strong donor such as EDOT, the HOMO-LUMO energy is increased compared to the TP-TP dimer. Of course, this effect would be even greater for comparably weaker donors, in which case the traditional donor would actually stabilize the D-A HOMO, rather than the desired destabilization. It is this effect that is believed to account for the reason that most TP-based D-A polymers exhibit higher bandgaps than TP homopolymers.[21]

Of particular interest, however, is the fact that the donor abilities of ambipolar units do provide opportunities for their non-traditional pairing with conventional acceptors. Comparison of EDOT-BTD and TP-BTD shows that the replacement of EDOT by TP results in essentially no change in the D-A HOMO, but a decrease in HOMO-LUMO energy due to LUMO stabilization. As such, this represents a completely new design paradigm for low E_g polymers via D-A frameworks, as recently demonstrated for TP-A polymers with bandgaps of 0.97-1.07 eV.[17,18]

Overall, the results confirm that D-A frameworks can be a powerful approach for the control of frontier orbitals and thus the reduction of HOMO-LUMO and/or bandgap energies. With that said, however, it is felt that the current understanding of D-A effects in conjugated materials is insufficient, regardless of the successful application of D-A frameworks to date. This is especially true in terms of our understanding of the electronic nature of building blocks applied to D-A frameworks and further characterization of common units is sorely needed, particularly for those that may possess ambipolar character. Such knowledge is critical to our ability to logically and purposefully design next-generation materials with desired energetic levels for specific applications.

Acknowledgements

The authors wish to thank Prof. Johannes Gierschner (IMDEA Nanoscience) for stimulating discussions. Thanks are also given to Merck Chemicals Ltd., the National Science Foundation (CHE-2002877), and North Dakota State University (NDSU) for support of this research, as well as to Dr. Angel Ugrinov (NDSU) for the collection of the X-ray crystal data, and NSFCRIF (CHE-0946990) for the purchase of the departmental XRD instrument. The work at the University of Málaga was financially supported by the MICINN (PID2019-110305GB-I00) and by the Junta de Andalucıa (P09-FQM-4708, UMA18-FEDERJA-080). The authors acknowledge the computer resources, technical expertise, and assistance provided by the SCBI (Supercomputing and Bioinformatics) centre of the University of Malaga.

Notes and references

This journal is © The Royal Society of Chemistry 20xx

Please do not adjust margins

Please do not adjust margins

1 S. C. Rasmussen, in *Handbook of Conducting Polymers*, 4th Ed, ed. J. R. Reynolds, T. A. Skotheim, and B. Thompson, CRC Press: Boca Raton, FL, 2019, pp. 1-35.
2 S. C. Rasmussen, *ChemPlusChem* 2020, **85**, 1412-1429.
3 *Handbook of Conducting Polymers*; 4th Ed, ed. J. R. Reynolds, T. A. Skotheim, and B. Thompson, CRC Press, Boca Raton, FL, 2019.
4 *Handbook of Thiophene-based Materials*, ed. I. F. Perepichka and D. F. Perepichka, John Wiley & Sons, Hoboken, 2009.
5 S. Günes, H. Neugebauer, and N. S. Sariciftci, *Chem. Rev.* 2007, **107**, 1324-1338.
6 A. C. Grimsdale, K. L. Chan, R. E. Martin, P. G. Jokisz, and A. B. Holmes, *Chem. Rev.*, 2009, **109**, 897-1091.
7 M. C. Scharber and N. S. Sariciftci, *Prog. Poly. Sci.*, 2013, **38**, 1929-1940.
8 C. B. Nielsen and I. McCulloch, *Prog. Poly. Sci.*, 2013, **38**, 2053-2069.
9 S. C. Rasmussen, S. J. Evenson, and C. B. McCausland, *Chem. Commun.*, 2015, **51**, 4528-4543.
10 J. Roncali, *Macromol. Rapid Commun.* 2007, **28**, 1761-1775.
11 S. C. Rasmussen, in *The Encyclopedia of Polymeric Nanomaterials*, ed. K. Muellen and S. Kobayashi, Springer, Heidelberg, 2015; pp 1155-1166.
12 S. C. Rasmussen and M. Pomerantz, in *Handbook of Conducting Polymers*, 3rd Ed., ed. T. A. Skotheim and J. R. Reynolds, CRC Press, Boca Raton, FL, 2007; Vol. 1, Chapter 12.
13 J. Gierschner, J. Cornil, and H.-J. Egelhaaf, *Adv. Mater.* 2007, **19**, 173-191.
14 M. Wykes, B. Milián-Medina, and J. Gierschner, *Front. Chem.* 2013, **1**, 35.
15 S. C. Rasmussen, R. L. Schwiderski, M. E. Mulholland, *Chem. Commun.* 2011, **47**, 11394-11410.
16 K. L. Konkol, R. L. Schwiderski, and S. C. Rasmussen, *Materials*, 2016, **9**, 404.
17 E. W. Culver, T. E. Anderson, J. T. L. Navarrete, M. C. R. Delgado, and S. C. Rasmussen. *ACS Macro Letters* 2018, **7**, 1215-1219.
18 T. E. Anderson, E. W. Culver, F. Almyahi, P. C. Dastoor, and S. C. Rasmussen. *Synlett* 2018, **29**(19), 2542-2546.
19 H. A. M. van Mullekom, J. A. J. M. Vekemans, E. E. Havinga, and E. W. Meijer, *Mater. Sci. Eng., R* 2001, **32**, 1-40.
20 E. Bundgaard, and F. C. Krebs, *Sol. Energy Mater. Sol. Cells* 2007, **91**, 954-985.
21 P. M. Beaujuge, C. M. Amb, and J. R. Reynolds, *Acc. Chem. Res.,* 2010, **43**, 1396-1407.
22 C. L. Chochos and S. A. Choulis, *Prog. Polym. Sci.*, 2011, **36**, 1326-1414.
23 C. Duan, F. Huang, and Y. Cao, *J. Mater. Chem.*, 2012, **22**, 10416-10434.
24 E. E. Havinga, W. ten Hoeve, and H. Wynberg, *Polym. Bull.,* 1992, **29**, 119-128.
25 E. E. Havinga, W. ten Hoeve, and H. Wynberg, *Synth. Met.,* 1993, **55**, 299-306.
26 M. Kertesz, C. H. Choi, and S. Yang, *Chem. Rev.*, 2005, **105**, 3448-3481.
27 U. Salzner, O. Karalti, and S. Durdagi, *J. Mol. Model.*, 2006, **12**, 687-701.
28 M. Kertesz, S. Yang, and Y. Tian, in *Handbook of Thiophene-Based Materials*, ed. I. F. Perepichka and D. F. Perepichka, John Wiley & Sons, Chichester, 2009, Vol. 1, pp. 341-364.
29 P. Ou, W. Shen, R. He, X. Xie, C. Zeng, and M. Li, *Polym. Int.,* 2011, **60**, 1408-1418.
30 A. D. Thilanga Liyanage, B. Milián-Medina, B. Zhang, J. Gierschner, and M. D. Watson, *Macromol. Chem. Phys.,* 2016, **217**, 2068-2073.
31 As proposed in the reference 30, the five general cases for the orbital diagram of D-A copolymers are: (1) HOMO and LUMO delocalized over both donor and acceptor groups; (2) HOMO delocalized over both donor and acceptor groups and LUMO localized on the acceptor; (3) HOMO localized on the donor and LUMO delocalized over both donor and acceptor groups; (4) HOMO localized on the donor and LUMO localized on the acceptor; and (5) HOMO and LUMO localized on the acceptor.
32 B. Milián-Medina and J. Gierschner, *Org. Elec.,* 2012, **13**, 985-991.
33 D. D. Kenning, K. A. Mitchell, T. R. Calhoun, M. R. Funfar, D. J. Sattler, and S. C. Rasmussen, *J. Org. Chem.*, 2002, **67**, 9073-9076.
34 S. C. Rasmussen, D. J. Sattler, K. A. Mitchell, and J. Maxwell, *J. Lumin.*, 2004, **190**, 111-119.
35 L. Wen, J. P. Nietfeld, C. M. Amb, and S. C. Rasmussen, *J. Org. Chem.* 2008, **73**, 8529-8536.
36 S. C. Rasmussen, M. E. Mulholland, R. L. Schwiderski, and C. A. Larsen. *J. Heterocyclic Chem.*, 2012, **49**, 479-493.
37 B. P. Karsten, L. Viani, J. Gierschner, J. Cornil, and R. A. J. Janssen, *J. Phys. Chem. A* 2008, **112**, 10764-10773.
38 L. Wen, C. L. Heth, and S. C. Rasmussen. *Phys. Chem. Chem. Phys.*, 2014, **16**, 7231-7240.
39 J. Roncali, P. Blanchard, and P. Frere, *J. Mater. Chem.,* 2005, **15**, 1589-1610.
40 Y. Wang and T. Michinobu, *J. Mater. Chem. C* 2016, **4**, 6200-6214.
41 J. Du, M. C. Biewer, and M. C. Stefan, *J. Mater. Chem. A,* 2016, **4**, 15771-15787.
42 M. Iyoda, H. Otsuka, K. Sato, N. Nisato, and M. Oda, *Bull. Chem. Soc. Jpn.*, 1990, **63**, 80-87.
43 K. Velauthamurty, R.M.G. Rajapakse, and S. J. Higgins, *Inorg. Chim. Acta,* 2017, **464**, 59-64.
44 P. Espinet and A. M. Echavarren, *Angew. Chem. Int. Ed.,* 2004, **43**, 4704-4734.
45 A. R. Katritzky and A. F. Pozharskii, *Handbook of Heterocyclic Chemistry*, 2nd Ed, Pergamon, New York, 2000, p 24, 61.
46 V. Luzzati, *Acta Crystallogr.* 1951, **4**, 193-200.
47 P. Pouzet, I. Erdelmeier, D. Ginderow, J.-P. Momon, P. M. Dansette, and D. Mansuy, *J. Heterocyclic Chem.*, 1997, **34**, 1567-1574.
48 *CRC Handbook of Chemistry and Physics*; Lide, D. R., Frederikse, H. P. R., Eds.; CRC Press: Boca Raton, FL, 1995; p 9-4.
49 J. A. R. P. Sarma and G. R. Desiraju, *Acc. Chem. Res.*, 1986, **19**, 222-228.
50 G. R. Desiraju, *Acc. Chem. Res.,* 1991, **24**, 290-296.
51 M. Mascal, *Chem. Commun.*, 1998, 303-304.
52 E. Bosch, *Cryst. Growth Des.,* 2010, **10**, 3808-3813.
53 A. V. Afonin, D. V. Pavlov, and A. V. Vashchenko, *J. Mol. Struct.,* 2019, **1176**, 73-85.
54 A. V. Afonin, A. V. Vashchenko, and H. Fujiwara, *Bull. Chem. Soc. Jpn.,* 1996, **69**, 933-945.
55 A. V. Afonin, A. V. Vashchenko, T. Takagi, A. Kimura, and H. Fujiwara, *Can. J. Chem.*, 1999, **77**, 416-424.
56 *Handbook of Chemistry and Physics*, 68th Ed., ed. R. C. Weast, CRC Press, Inc., Boca Raton, 1987, p. D-188.
57 Y. A. Getmanenko, S. Singh, B. Sandhu, C.-Y. Wang, T. Timofeeva, B. Kippelen, and S. R. Marder, *J. Mater. Chem. C,* 2014, **2**, 124-131.
58 E. J. Uzelac, C. B. McCausland, and S. C. Rasmussen, *J. Org. Chem.,* 2018, **83**, 664-671.
59 N. J. Turro, Modern Molecular Photochemistry, University Science Books: Sausalito, CA, 1991; pp 105-110.
60 C. M. Cardona, W. Li, A. E. Kaifer, D. Stockdale, and G. C. Bazan, *Adv. Mater.,* 2011, **23**, 2367-2371.
61 L. Dou, Y. Liu, Z. Hong, G. Li, and Y. Yang. *Chem. Rev.*, 2015, **115**, 12633-12665.
62 A. Ajayaghosh, *Chem. Soc. Rev.,* 2003, **32**, 181-191.
63 S. J. Evenson, M. E. Mulholland, T. E. Anderson, and S. C. Rasmussen, *Asian J. Org. Chem.,* 2020, **9**, 1333-1339.
64 Y.-M. Tao, H.-Y. Li, Q.-L. Xu, Y.-C. Zhu, L.-C. Kang, Y.-X. Zheng, J.-L. Zuo, and X.-Z. You, *Synth. Met.,* 2011, **161**, 718-723. **[66]**

Please do not adjust margins

Please do not adjust margins

65 M. Belletete, S. Beaupre, J. Bouchard, P. Blondin, M. Leclerc, and G. Durocher, *J. Phys. Chem. B,* 2000, **104**, 9118-9125.
66 K. Pilgram, M. Zupan, and R. Skiles, *J. Heterocycl. Chem.,* 1970, **7**, 629-633.
67 J. W. Zubrick, *The Organic Chem Lab Survival Manual*, 10th Ed, John Wiley & Sons, Hoboken, 2015, pp 168-172.
68 T. Fukushima, N. Okazeri, T. Miyashi, K. Suzuki, Y. Yamashita, and T. Suzuki, *Tetrahedron Lett.,* 1999, **40**, 1175-1178.
69 P. Anant, N. T. Lucas, and J. Jacob, *Org. Lett.,* 2008, **10**, 5533-5536.
70 E. Xu, H. Zhong, J. Du, D. Zeng, S. Ren, J. Sun, and Q. Fang, *Dyes Pigm.,* 2009, **80**, 194-198.
71 G. A. Sotzing, J. R. Reynolds, and P. J. Steel, *Adv. Mater.*, 1991, **9**, 795-798.
72 M. J. Frisch, G. W. Trucks, H. B. Schlegel, G. E. Scuseria, M. A. Robb, J. R. Cheeseman, G. Scalmani, V. Barone, G. A. Petersson, H. Nakatsuji, X. Li, M. Caricato, a. V. Marenich, J. Bloino, B. G. Janesko, R. Gomperts, B. Mennucci, H. P. Hratchian, J. V. Ortiz, A. F. Izmaylov, J. L. Sonnenberg, Williams, F. Ding, F. Lipparini, F. Egidi, J. Goings, B. Peng, A. Petrone, T. Henderson, D. Ranasinghe, V. G. Zakrzewski, J. Gao, N. Rega, G. Zheng, W. Liang, M. Hada, M. Ehara, K. Toyota, R. Fukuda, J. Hasegawa, M. Ishida, T. Nakajima, Y. Honda, O. Kitao, H. Nakai, T. Vreven, K. Throssell, J. A. Montgomery Jr., J. E. Peralta, F. Ogliaro, M. J. Bearpark, J. J. Heyd, E. N. Brothers, K. N. Kudin, V. N. Staroverov, T. A. Keith, R. Kobayashi, J. Normand, K. Raghavachari, A. P. Rendell, J. C. Burant, S. S. Iyengar, J. Tomasi, M. Cossi, J. M. Millam, M. Klene, C. Adamo, R. Cammi, J. W. Ochterski, R. L. Martin, K. Morokuma, O. Farkas, J. B. Foresman and D. J. Fox, 2016, Gaussian 16, Revision C.01, Gaussian, Inc., Wallingford CT.
73 E. Runge and E. K. U. Gross, *Phys. Rev. Lett.* 1984, **52**, 997-1000.
74 M. E. Casida, in *Recent Advances in Density Functional Methods, Part I*, ed. D. P. Chong, World Scientific Publishing, Singapore, 1995, p. 155.
75 A. D. Becke, *J. Chem. Phys.,* 1993, **98**, 5648-5652.
76 C. T. Lee, W. T. Yang and R. G. Parr, *Phys. Rev. B: Condens. Matter Mater. Phys.*, 1988, **37**, 785.
77 J.-D. Chai and M. Head-Gordon, *J. Chem. Phys.*, 2008, **128**, 084106–084115.
78 L. Pandey, C. Doiron, J. S. Sears and J.-L. Brédas, *Phys. Chem. Chem. Phys.*, 2012, **14**, 14243–14248
79 A. D. McLean and G. S. Chandler, *J. Chem. Phys.,* 1980, **72**, 5639.
80 R. Krishnan, J. S. Binkley, R. Seeger, and J. A. People, *J. Chem. Phys.*, 1980, **72**, 650.
81 Chemcraft - graphical software for visualization of quantum chemistry computations. https://www.chemcraftprog.com.
82 N. J. Turro, *Modern Molecular Photochemistry*, University Science Books: Sausalito, CA, 1991; pp 86-90.
83 R. C. Larson, R. T. Iwamoto, and R. N. Adams, *Anal. Chim. Acta* 1961, **25**, 371-374.

This journal is © The Royal Society of Chemistry 20xx

Please do not adjust margins